

Electronic resonant states of HCO and HOC

Å. Larson*

Department of Physics, Stockholm University, AlbaNova University Center, S-106 91 Stockholm, Sweden

A. E. Orel

Department of Applied Science, University of California, Davis, California 95616, USA

(Received 7 September 2009; published 4 December 2009)

The electronic resonant states of HCO and HOC are calculated using the complex Kohn variational method combined with structure calculations using multireference configuration interaction. No resonant state of HCO crosses the ion potential close to its minimum. Several resonances at higher energies are observed. There are clear indications of avoided crossings between the resonant states. There are resonant states that are repulsive with respect to both radial coordinates, but they remain relatively unchanged in energy as a function of the bending angle. For HOC, there are a manifold of resonant states with similar shapes as the potentials of HCO. However, the resonant states of HOC are lower in energy relative to the ion and could play an important role for dissociative recombination of HOC⁺ at low collision energies.

DOI: [10.1103/PhysRevA.80.062504](https://doi.org/10.1103/PhysRevA.80.062504)

PACS number(s): 31.50.Df, 34.80.Lx, 34.80.Ht

I. INTRODUCTION

The formyl cation, HCO⁺, is one of the most important molecular ions of interstellar chemistry. The first rotational line ever observed of a molecule in interstellar space was the so-called X-ogen line at 89.190 GHz detected in 1970 by Buhl and Snyder [1]. The line was assigned to the $J=1-0$ transition of HCO⁺ [2]. The HCO⁺ ion is the most abundant ion detected so far by radio astronomical observations [3]. It is believed to be formed mainly by proton transfer between H₃⁺ and CO [4]. In interstellar space, the destruction of HCO⁺ is dominated by dissociative recombination (DR), where the ion captures a low energetic electron, forming a neutral state that stabilizes through dissociation into fragments. The first measurement of dissociative recombination of HCO⁺ was performed as early as 1973 by Leu *et al.* [5] using a microwave afterglow technique combined with a mass spectrometer apparatus. The first laboratory microwave spectrum of HCO⁺ was published in 1975 by Woods *et al.* [6].

The study of dissociative recombination of the HCO⁺ ion has a long history, both experimentally and theoretically. After the measurement by Leu *et al.* [5], there have been numerous experiments on dissociative recombination of HCO⁺ not only using stationary afterglows [7,8], but also flowing afterglows [9–19], a merged-beam study [20], as well as more recent ion-storage ring experiments [21]. These measurements agree on a relative large DR rate of around $2 \times 10^{-7} \text{ cm}^3 \text{ s}^{-1}$ at 300 K, but the temperature dependence of the measured rates varies in the different experiments. Measurements of the branching ratios show that in this reaction the HC bond will break [11,21]. Furthermore, analysis of the CO band emissions shows that DR of HCO⁺ forms the long-lived CO(*a* ³Π) state with a yield of 0.23 ± 0.12 [18]. The vibrational distribution of the CO fragment has also been measured [12,15]. All these experiments have been carried out at low collision energies. Some preliminary measure-

ments using the CRYRING ion-storage ring [22] indicate that at higher energies, between 3 and 10 eV, there is a structured peak in the cross section. Similar high-energy peaks have been observed for numerous molecular ions, both polyatomic systems such as H₃⁺ and CO₂⁺ as well as diatomic systems such as HD⁺ and HeH⁺ (see [23] and references therein).

The first theoretical study of the electronic states relevant in dissociative recombination of HCO⁺ was in 1985 by Kraemer and Hazi [24,25]. Using the complete active space self-consistent field method, structure calculations were carried out at linear geometry on the ground state of the HCO⁺ ion and some of the excited states of HCO. No indications were found of a neutral state crossing the ionic ground-state potential close to its minimum. This type of curve crossing is needed in order to have a “direct mechanism” of dissociative recombination, first proposed by Bates [26]. However, the theoretical studies carried out by Talbi *et al.* [27,28] revealed a curve crossing close to the equilibrium geometry of the ground ionic state. Talbi *et al.* calculated the adiabatic potentials at linear geometry using the configuration-interaction (CI) method with projected localized orbitals. By applying a diabaticization procedure, a quasidiabatic potential was found to cross the ionic ground-state potential close to its minimum. Bates did not believe in the crossing potentials calculated by Talbi. Instead, he suggested a multistep mechanism through vibrational excited Rydberg states to explain the relative high measured DR rate of HCO⁺ [29].

Using the multireference configuration-interaction (MRCI) method with a very large basis set, the excited-state potential surfaces of HCO were calculated by Larson *et al.* [30]. It was found that no neutral potential curve crosses the ion potential close to its minimum. The DR of HCO⁺ at low energies was suggested to be driven by the electron capture into the Rydberg states situated below the ion. Using the multichannel quantum defect theory (MQDT), the Renner-Teller effect that couples the electronic and nuclear degrees of freedom of the system was found to be important to include in the theoretical model [31]. The calculated DR rate was a factor of 2–3 smaller than the measured rates. In [31]

*Corresponding author; aasal@physto.se

the CO bond length was frozen at its equilibrium distance. In the next step [32] the CO bond length was allowed to vibrate. However, this only affected the calculated cross section above 0.1 eV, when the electron has enough energy to vibrationally excite the CO motion. By fitting spectroscopic data, the Renner-Teller parameters of HCO have been extracted and by using a simple model it was confirmed that the coupling due to Renner-Teller interaction is largely responsible for the DR cross section at low energies [33]. Very recently [34], a generalized MQDT treatment has been applied where also the considerable permanent dipole moment ($\mu \approx 4$ D) of the HCO⁺ ion has been included. This causes an increase in the cross section of about 50%.

The isoformyl molecular ion, HOC⁺, is an isomer of HCO⁺ that is situated about 13 900 cm⁻¹ (1.72 eV) higher in energy and with a barrier to isomerization of 13 000 cm⁻¹ (1.61 eV) [35]. The first spectroscopic detection of the HOC⁺ ion was made in 1982 by laboratory microwave techniques [36]. Since then, it has been observed in interstellar environments in both dense [37,38] and diffuse [39] molecular clouds. The interstellar abundance ratio [HCO⁺]/[HOC⁺] has been discussed and is believed to vary between 70–360 [38,39]. This ion is also believed to be formed by proton transfer in collisions with H₃⁺ and CO. In diffuse clouds, it can also be formed by the reaction C⁺+H₂O→HOC⁺+H₂. It has been postulated that the main destruction mechanism of HOC⁺ is by collisions with H₂, i.e., HOC⁺+H₂→HCO⁺+H₂. Another competing destruction path is by dissociative recombination with low-energy electrons.

Using a flowing afterglow experiment [18] evidence was found that in the plasma both isomers HCO⁺ and HOC⁺ can be formed. By analyzing the CO band emission, it was found that the excited states of CO are formed [CO(*a'* ³Σ⁺) and CO(*d* ³Δ)] with a combined yield of greater than 0.4 in dissociative recombination of HOC⁺. However, as far as we know, there is no experimental or theoretical determination of the DR rate coefficient of HOC⁺. When modeling the chemistry of the afterglow plasma [18], it was assumed that the DR thermal rate coefficients of HCO⁺ and HOC⁺ are of the same magnitude. For the models of the interstellar chemistry it is assumed that the thermal DR rate coefficient of HOC⁺ is 1.3×10^{-7} cm³ s⁻¹ [19,39,40].

In the experiments on DR of HCO⁺, the HOC⁺ ion could also be formed. The two isomers can be difficult or even impossible to separate [19]. Assume that the two isomers have DR cross sections with different magnitudes, for example, the cross section for HOC⁺ can be larger than the cross section for HCO⁺ at low energies. Then this might help to explain the difference in magnitude of the measured and calculated cross sections for DR of HCO⁺.

In the present study we calculate the electronic resonant states of HCO and HOC. These states are above the ion potential in energy and they interact with the ionization continuum. Therefore, they are not true bound states of the system and we carry out electron-scattering calculations using the complex Kohn variational method [41] to describe these states. Using this method both the energy positions and the autoionization widths of the resonant states can be determined. These electron-scattering calculations are carried out at linear geometry and as a function of the two bond lengths.

The resonant states are followed when they cross the ion and interact with the Rydberg manifold below the ion by performing MRCI calculations that are consistent with the target functions used with the electron-scattering calculations. The MRCI calculations are also carried to examine the angle dependence of the resonant states in the Franck-Condon region. In the present study we can finally establish whether or not there is a curve crossing of the HCO resonant state with the ion potential close to the equilibrium structure. Furthermore, we will be able to examine if the resonant states can explain the high-energy peak observed in the measured cross section using the CRYRING ion-storage ring [22]. We also calculate the resonant states of HOC in order to determine the mechanism for DR of HOC⁺. Here, both the energy positions and autoionization width of the resonant states are computed. In a later study, the dynamics on these resonant states will be carried out in order to calculate DR cross sections.

The outline of this paper is as follows. In Sec. II we describe how the theoretical calculations of the resonant states are carried out by combining structure calculations (Sec. II A) with electron-scattering calculations (Sec. II B). This is followed by a quasidiabatization (Sec. II C) where the resonant states are extracted from the structure data. The resulting potential-energy surfaces of HCO and HOC are shown in Sec. III. This is followed by a discussion of the role of the resonant states for DR of HCO⁺ and HOC⁺ in Sec. IV. Atomic units will be used throughout the paper.

II. THEORETICAL DETAILS

A. Structure calculations

The potential-energy surfaces of the ion as well as excited states of the neutral molecule are calculated using the MRCI method. This will provide us with the potential energy of the electronically bound states that are situated below the ground state of the ion. We also use the structure calculations to interpolate the potentials of the resonant states between the geometries where electron-scattering calculations are performed. Furthermore, structure calculations are carried out for bent geometries of the molecule. When the molecule becomes bent, the $C_{\infty v}$ symmetry becomes C_s and a larger CI calculation is needed as more configurations begin to interact. The electron-scattering calculations at bent geometries are too time consuming and therefore structure calculations are carried out in order to determine the shape of the resonant state potentials as a function of the bending angle.

The structure calculations start with a self-consistent field calculation on the ion. For the hydrogen atom, a basis set of (4*s*, 1*p*) contracted to [3*s*, 1*p*] is used. For the carbon atom, the basis consists of (9*s*, 6*p*, 1*d*) contracted to [5*s*, 4*p*, 1*d*], while (9*s*, 7*p*, 1*d*) contracted to [4*s*, 4*p*, 1*d*] is used for the oxygen atom. In the next step, natural orbitals are extracted from a configuration-interaction calculation on the ground state X ¹Σ⁺ of the ion, where single and double excitations out of the ground-state configuration are included. The natural orbitals are then further expanded by adding diffuse (1*s*, 1*p*) orbitals on carbon and oxygen and (2*s*, 2*p*) on hydrogen.

Then a MRCI calculation is applied to determine the potential-energy surfaces of the ground state of the ion as well as excited states of the neutral molecule. In these calculations, the two lowest $(1\sigma)(2\sigma)$ core orbitals are kept doubly occupied and the reference configurations are constructed by excitations of 11 electrons (ten for the ion) among the eight orbitals: $(3\sigma)(4\sigma)(5\sigma)(1\pi)(2\pi)(6\sigma)$. Single excitations out of the reference configurations are included. For the HCO system, structure calculations are carried out at 58 geometries where the CO distance ranged from $1.5a_0$ to $4.0a_0$ and the HC distance from $1.0a_0$ to $5.0a_0$. The angle is varied from 0° (linear geometry) to 20° . For the HOC system, structure calculations are carried out at 50 geometries where the OC distance ranged from $1.5a_0$ to $4.0a_0$ and the HO distance from $1.0a_0$ to $4.0a_0$. Again the potentials are calculated as a function of the bending angle between 0° and 20° .

B. Scattering calculations

By using the complex Kohn variational method [41], the energy positions and autoionization widths of the electronic resonant states can be determined. As a target wave function Φ_i , the same MRCI wave function for the ion as used in the structure calculations is employed. In the complex Kohn variational method, the trial wave function for the neutral $(N+1)$ electron system is written as

$$\Psi = \sum_i A[\Phi_i(\mathbf{r}_1, \dots, \mathbf{r}_N)F_i(\mathbf{r}_{N+1})] + \sum_\mu d_\mu \Theta_\mu(\mathbf{r}_1, \dots, \mathbf{r}_{N+1}). \quad (1)$$

The first sum is denoted as the P -space portion of the wave function and runs over the energetically open target states. In the present study, only the ground ionic state is included. We can therefore only determine resonant states below the first excited state of the ion. The function $F_i(\mathbf{r}_{N+1})$ is the one-electron wave function describing the scattered electron and A is an antisymmetrization operator for the electronic coordinates. The second term, denoted as the Q -space portion of the wave function, contains the functions Θ_μ , which are square-integrable $N+1$ configuration state functions that are used to describe short-range correlations and the effects of closed channels. We use the same natural orbitals as those applied in the structure calculations described in the previous section. The advantage of using natural orbitals is that the orbital space used to generate these states is kept manageable small. The one-electron-scattering wave function F_i is in the case of electron-ion scattering further expanded as

$$F_i(\mathbf{r}) = \sum_j c_j^i \phi_j(\mathbf{r}) + [f_l^-(k_i r) \delta_{l_0} \delta_{mm_0} + T_{l_0 q m m_0}^i f_l^+(k_i r)] Y_{lm}(\hat{\mathbf{r}})/r. \quad (2)$$

Here, $\phi_j(\mathbf{r})$ are a set of square-integrable functions, f_l^\pm are the outgoing and incoming Coulomb functions, and Y_{lm} are spherical Harmonics. Angular momenta up to $l=6$ and $|m|=4$ are included in the calculation.

By inserting the trial wave function into the complex Kohn functional [41], the unknown coefficients in the trial wave function can be optimized. Then also the T matrix ($T_{l_0 q m m_0}^i$) for elastic scattering is obtained, and by fitting the eigenphase sum of the T matrix to a Breit-Wigner form [42], the energy positions and autoionization widths of the resonant states are determined. These electron-scattering calculations are carried out for a fixed geometry of the target ion. The electron-scattering calculations are carried out at linear geometries only and three resonant states of $^2\Sigma^+$ and $^2\Delta$ symmetries and four states of $^2\Pi$ symmetry are computed. Electron-scattering calculations are carried out for 14 different geometries of the HCO system, where the CO distance varies from $1.8a_0$ to $2.5a_0$ and the HC distance from $1.5a_0$ to $3.0a_0$. For the HOC system, the scattering calculations are carried out at the same corresponding geometries.

C. Quasidiabatization

Both the HCO⁺ and HOC⁺ molecular ions have linear equilibrium geometries in their ground states. For HCO⁺, the $\tilde{X}^1\Sigma^+$ state has the equilibrium bond lengths $R_{HC}=2.046a_0$ and $R_{CO}=2.099a_0$. The ground state of HOC⁺, $\tilde{X}^1\Sigma^+$, has the equilibrium bond lengths $R_{HO}=1.867a_0$ and $R_{OC}=2.182a_0$ [43]. The ionic ground states are dominated by the configuration $(1\sigma)^2(2\sigma)^2(3\sigma)^2(4\sigma)^2(5\sigma)^2(1\pi)^4$. When structure calculations are carried out, three types of states are obtained. These are the Rydberg states converging to the ground ionic cores, the states trying to describe the ionization continuum, as well as the resonant states. Both the Rydberg states as well as the states describing the ionization continuum have the same configuration as the ground state of the ion plus an outer electron in a diffuse orbital. The resonant states are more or less compact Rydberg states converging to excited ionic cores. These resonant states all have a vacancy in either the (5σ) or the (1π) molecular orbitals. By following the states with this character, the resonant states can be “diabatized” relative to the Rydberg states and the ionization continuum. This is done in order to follow the resonant states when they cross the ionic ground state and interact with the Rydberg manifold situated below the ionic potential. We also use this approach to obtain more data for the potential-energy surfaces of the resonant states above the ion and interpolate and extrapolate between the resonant states calculated using the electron-scattering formalism. It should be noted that this approach will provide us with the position of the resonant state within the energy spread given by the autoionization width. The HCO and HOC systems have resonant states that are very narrow, and hence the use of structure data to obtain resonant states is relatively accurate. We have only diabated the resonant states relative to the Rydberg states by using the CI coefficients. We have not calculated any electronic couplings between the neutral states. In addition, we have not diabated the resonant states among each other. As will be shown below, there are clear indications of avoided crossings among the resonant states.

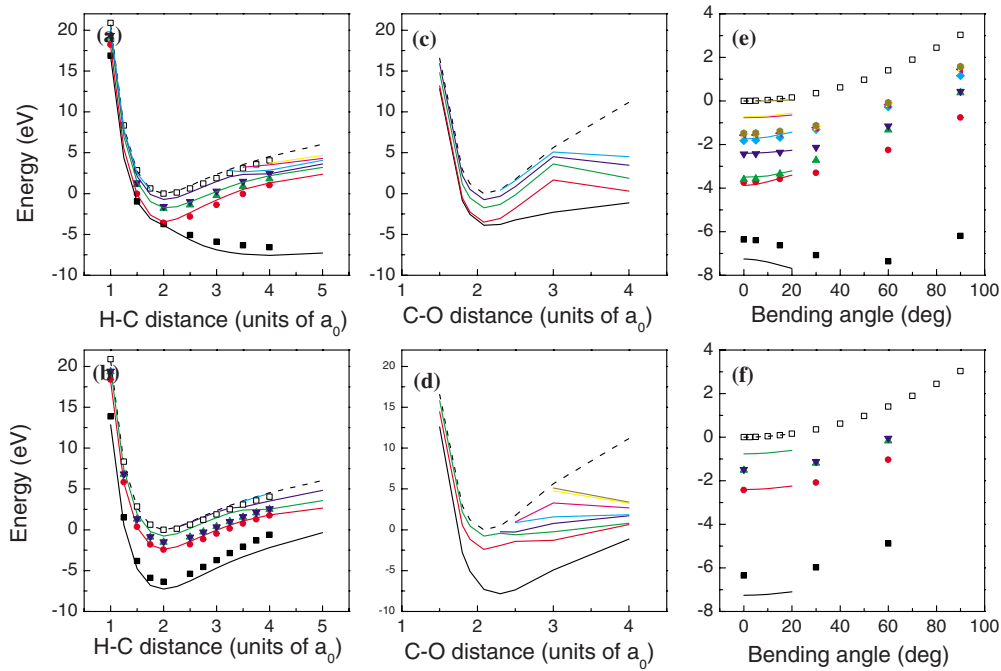


FIG. 1. (Color online) Ground-state potential of the HCO^+ ion and adiabatic neutral states situated below the ion potential as a function of the three internal coordinates. In (a) and (b), the potential-energy surfaces of $^2\Sigma^+$ and $^2\Pi$ symmetries are displayed as a function of the R_{HC} coordinate. The lines are the potentials from the present study (where $R_{\text{CO}}=2.08a_0$ and $\theta=0^\circ$), while symbols are potentials calculated by Larson *et al.* [30] (with $R_{\text{CO}}=2.0877a_0$ and $\theta=0^\circ$). The potential of the ion is shown with dashed line (open symbols). The potentials are shifted relative to the minimum of the ion. In (c) and (d) the $^2\Sigma^+$ and $^2\Pi$ potential-energy surfaces are displayed as a function of the R_{CO} coordinate (with $R_{\text{HC}}=2.0a_0$ and $\theta=0^\circ$), while in (e) and (f) the potential-energy surfaces of $^2A'$ and $^2A''$ symmetries are shown as a function of the bending angle for fixed radial coordinates ($R_{\text{HC}}=2.0a_0$ and $R_{\text{CO}}=2.08a_0$). The symbols show the potential surfaces calculated by Larson *et al.* [30] at $R_{\text{HC}}=2.0a_0$ and $R_{\text{CO}}=2.0877a_0$.

III. RESULTS

We show slices of the calculated potential-energy surfaces of HCO and HOC. For the HCO system, we first show the calculated adiabatic potentials situated below the ion, obtained directly from the structure calculations. We then display energies and autoionization widths of the resonant states of HCO and HOC [44].

A. Electronic states of HCO

1. Adiabatic potentials

Using the MRCI technique as described in Sec. II A, the adiabatic potentials situated below the ionic ground state have been calculated. In order to test the accuracy of the present calculations, the potentials are compared with the very accurate MRCI calculations by Larson *et al.* [30]. It should be noted that since we need to combine the structure calculations with electron-scattering calculations carried out at the same level of theory, the scattering calculations will limit the size of the structure wave functions. Therefore, the potential curves calculated by Larson *et al.* will be lower in the total energy compared to the present potentials. We have shifted all potentials relative to the minimum of the ion. This corresponds to a shift of the potential surfaces by Larson *et al.* by -113.35616 hartree and the present potentials are shifted by -113.1347 hartree. In the previous calculations, a

very large diffuse basis set was used in order to accurately describe the Rydberg states. Therefore, we will not obtain all Rydberg states seen in the previous calculation. The focus of the present study is the resonant states, and we believe that we have a good description of these more compact states.

In Fig. 1, we show slices of the calculated adiabatic potentials of HCO as a function of the three internal coordinates. In Figs. 1(a) and 1(b), the potentials of $^2\Sigma^+$ and $^2\Pi$ symmetries are shown as a function the H-C radial coordinate, where the other two internal coordinates are frozen at $\theta=0^\circ$ and $R_{\text{CO}}=2.08a_0$. The two studies show similar avoided crossings between the two lowest states of $^2\Sigma^+$ symmetry. Furthermore, the present study show clear indications of avoided crossings around $R_{\text{HC}}\approx 3.5a_0$ where the resonant states cross the ion and start to interact with the Rydberg manifold. The states of $^2\Pi$ symmetry show no indications of avoided crossings at small internuclear distances, only around $R_{\text{HC}}=3.5a_0$. It should be noticed that the present study is not able to calculate the $3d\sigma$ and $3d\pi$ Rydberg states observed in the previous study.

In Figs. 1(c) and 1(d), the adiabatic potentials are displayed as a function of the C-O coordinate for fixed $R_{\text{HC}}=2.0a_0$ and $\theta=0^\circ$. There are changes in slopes of the potentials at larger distances, indicating interactions between Rydberg states and repulsive resonant states. In the previous study [30], the potential-energy surfaces were not calculated

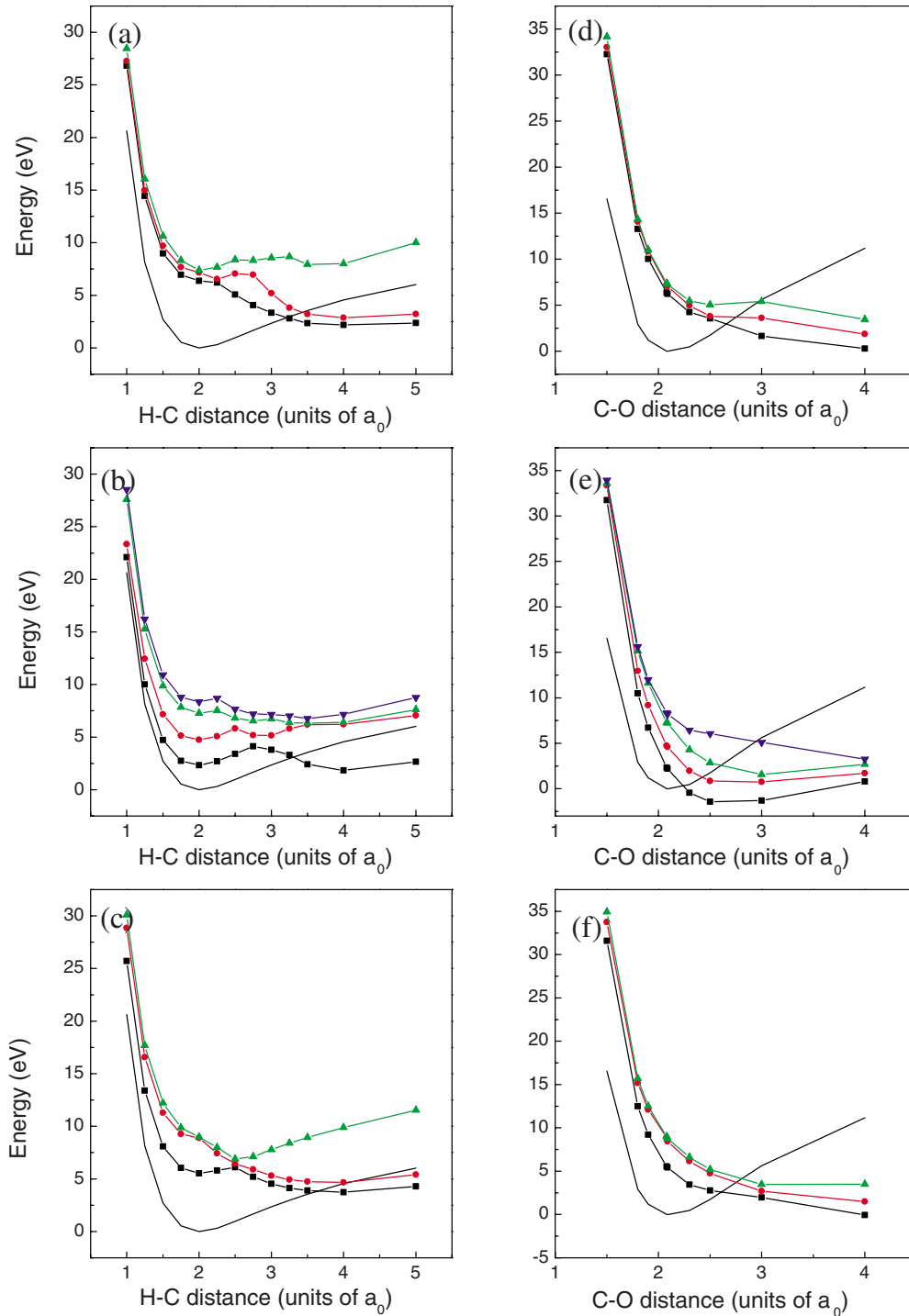


FIG. 2. (Color online) Resonant states of HCO of ${}^2\Sigma^+$, ${}^2\Pi$, and ${}^2\Delta$ symmetries. In (a)–(c) the potential-energy surfaces are plotted as a function of the R_{HC} coordinate with $R_{CO}=2.08a_0$ and $\theta=0^\circ$ fixed, while in (d)–(f) the surfaces are plotted as a function of the R_{CO} coordinate (with $R_{HC}=2.0a_0$ and $\theta=0^\circ$ frozen). The potential of the ion is displayed with the solid curve.

(with the MRCI method) as a function of the C-O coordinate.

In the studies on DR of HCO^+ [30–32] much focus has been on the angle dependence of the potentials surfaces of the Rydberg states of HCO. This angle dependence will determine the Renner-Teller coupling strength that is found to be important in the low-energy DR. In Figs. 1(e) and 1(f), the potential-energy surfaces of the electronic states situated below the ground state of the ion are plotted as a function of

the bending angle and for fixed bond lengths of $R_{CO}=2.08a_0$ and $R_{HC}=2.0a_0$. Again, we compare the potentials from the present study with those calculated by Larson *et al.* [30]. Here, we have only calculated the potentials when the angle θ goes from 0° to 20° , while in the previous study, the bending angle went all the way to 90° . The present study show similar angle dependence of the Rydberg states as found in the previous study.

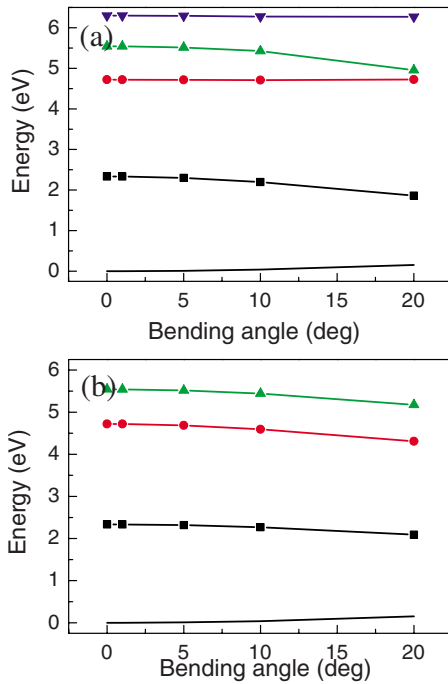


FIG. 3. (Color online) Resonant states of HCO of (a) ${}^2A'$ and (b) ${}^2A''$ symmetries as a function of the bending angle and for fixed radial coordinates ($R_{HC}=2.0a_0$ and $R_{CO}=2.08a_0$). Also the ground state, $X\ {}^2A'$, of the HCO^+ ion is shown with the solid curve.

2. Resonant states

By carrying out electron-scattering calculations and combining these with the structure calculations, we can extract potential-energy surfaces of the resonant states of HCO. We calculate three resonant states of ${}^2\Sigma^+$ symmetry, three of ${}^2\Delta$, and four of ${}^2\Pi$ symmetry. As described above, the resonant states are diabaticized relative to the Rydberg states converging to the ground ionic core. The resonant states are however not diabaticized relative to each other. In Fig. 2, we display the HCO resonant states of ${}^2\Sigma^+$, ${}^2\Pi$, and ${}^2\Delta$ symmetries as a function of the two radial coordinates.

We do not obtain any resonant states that cross the ionic ground-state potential close to its minimum. We obtain several resonant states at higher energies. At the equilibrium geometry of the ion, the lowest resonant state is a ${}^2\Pi$ state situated about 2.21 eV above the ion potential. The energy of the lowest ${}^2\Sigma^+$ resonant state is 6.23 eV, while the lowest ${}^2\Delta$ resonant state is about 5.44 eV above the ion.

As a function of the H-C coordinate, the resonant states show clear indications of avoided crossings between bound and dissociative resonant states. Similar avoided crossings are found among the potential-energy surfaces of excited ionic states. Since the resonant states are Rydberg states that converge to the excited ionic cores, the same behavior of the potentials are found for the resonant states. The repulsive resonant states cross the ion potential at larger internuclear distances ($R_{HC}\approx 3.2a_0$ for ${}^2\Sigma^+$ and ${}^2\Pi$ resonant states and $R_{HC}\approx 3.7a_0$ for the ${}^2\Delta$ states). At larger internuclear distances, they will start to interact with the Rydberg states situated below the ion, as described in the previous section.

As displayed in Figs. 2(d)–2(f), all resonant states of ${}^2\Sigma^+$, ${}^2\Pi$, and ${}^2\Delta$ symmetries are repulsive as a function of the C-O

TABLE I. Autoionization widths of the resonant states of HCO at $R_{HC}=2.0a_0$, $R_{CO}=2.08a_0$, and $\theta=0^\circ$.

Resonant state	Autoionization width (eV)
1 ${}^2\Sigma^+$	0.027
2 ${}^2\Sigma^+$	0.020
3 ${}^2\Sigma^+$	0.010
1 ${}^2\Pi$	0.036
2 ${}^2\Pi$	0.016
3 ${}^2\Pi$	0.25
4 ${}^2\Pi$	0.020
1 ${}^2\Delta$	0.0073
1 ${}^2\Delta$	0.056
1 ${}^2\Delta$	0.085

coordinate. The lowest ${}^2\Sigma^+$ resonant state crosses the ion potential around $R_{CO}\approx 3.6a_0$, while for ${}^2\Pi$ and ${}^2\Delta$, the crossings occur at $2.2a_0$ and $2.6a_0$.

In Fig. 3, the resonant states of ${}^2A'$ and ${}^2A''$ symmetries are plotted as a function of the bending angle. The first point ($\theta=0^\circ$) of the potential-energy surfaces of the resonant states are obtained from electron-scattering calculation in C_{2v} symmetry, while the remaining points on the slices of the potential-energy surfaces are from structure calculations using C_s symmetry. As a function of the bending coordinate, the resonant states are relatively flat in the Franck-Condon region.

The electron-scattering calculations do not only provide us with the energy positions of the resonant states, but also the autoionization widths. The autoionization widths of the resonant states of HCO are relatively small. In Table I, the magnitudes of the widths of the resonant states close to the equilibrium geometry ($R_{HC}=2.0a_0$ and $R_{CO}=2.08a_0$) are listed. In the Franck-Condon region, most of the autoionization widths are relatively independent on changes in the internuclear coordinates. However, some of the widths increase in the region where the potential of the resonant state crosses the ion potential. This is the case for the widths of the $2\ {}^2\Sigma^+$ and $1\ {}^2\Pi$ states that reach a magnitude of about 0.26 eV when the resonant state potentials cross the ion potential.

B. Electronic states of HOC

Resonant states

The resonant states of HOC are calculated using the same method used for HCO. We have calculated three resonant states of ${}^2\Sigma^+$ and ${}^2\Delta$ symmetries and four states of ${}^2\Pi$ symmetry. In Fig. 4, the resonant states of HOC of ${}^2\Sigma^+$, ${}^2\Pi$, and ${}^2\Delta$ symmetries are shown as a function of the two radial coordinates. The energies of all potentials are shifted relative to the minimum of the ion. The resonant states of HOC are much lower in energy relative the ion compared to HCO. The lowest resonant state is a ${}^2\Delta$ state, which is 0.23 eV above the ion at the equilibrium structure. The lowest ${}^2\Sigma^+$ resonant state is about 0.84 eV above the ion, while the lowest resonant state of ${}^2\Pi$ symmetry is 3.58 eV above the ion potential

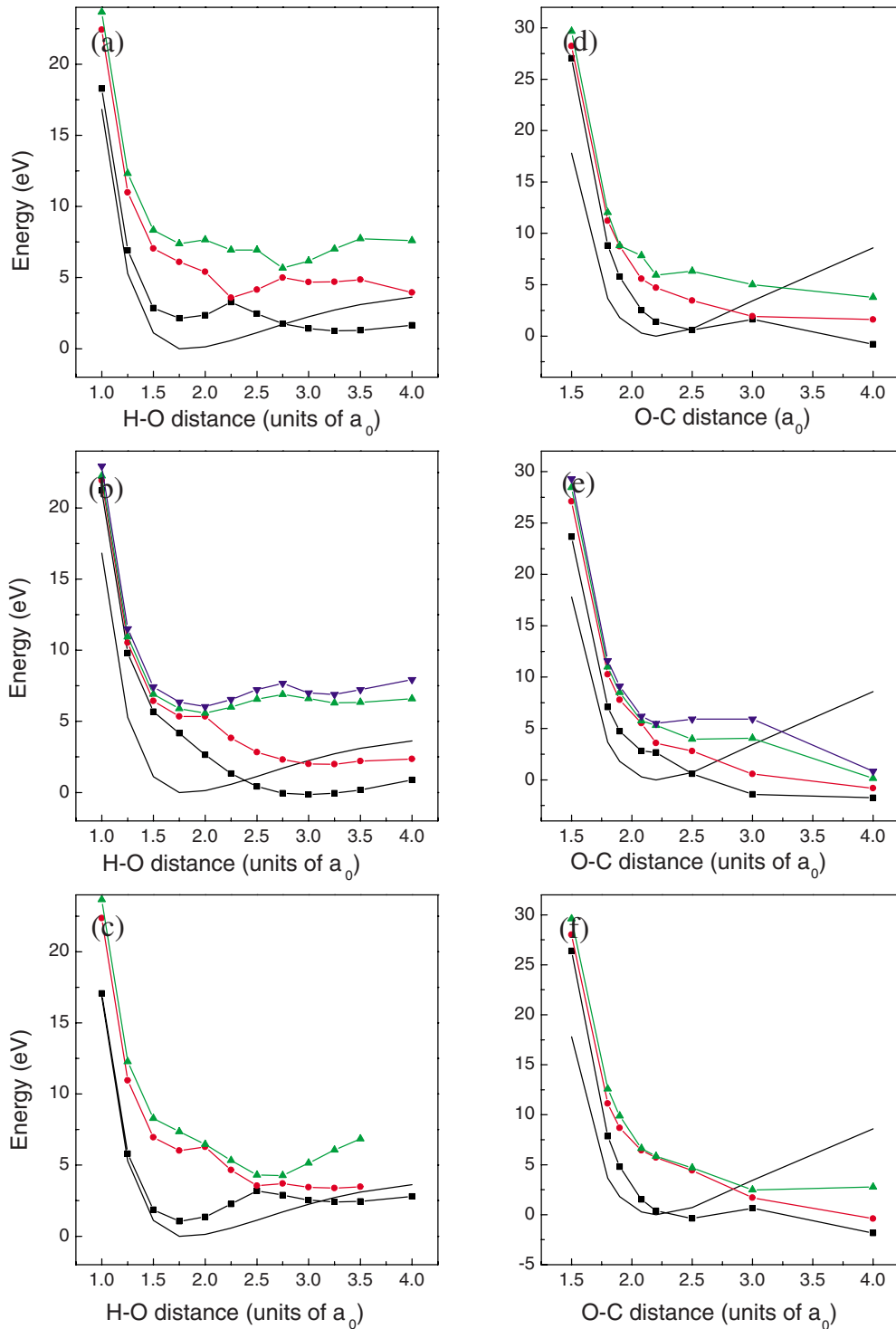


FIG. 4. (Color online) Resonant states of HOC of ${}^2\Sigma^+$, ${}^2\Pi$, and ${}^2\Delta$ symmetries. In (a)–(c) the potential-energy surfaces are plotted as a function of the R_{HO} coordinate with $R_{OC}=2.08a_0$ and $\theta=0^\circ$ fixed, while in (d)–(f) the surfaces are plotted as a function of the R_{OC} coordinate (with $R_{HO}=2.0a_0$ and $\theta=0^\circ$ frozen). The potential of the ion is displayed with the solid curve.

(calculated at $R_{HO}=1.75a_0$ and $R_{OC}=2.2a_0$). As a function of the H-O coordinate, there are bound resonant states interacting with repulsive states, creating avoided crossings among the resonant states.

As a function of the O-C coordinate the resonant states are repulsive; however, in the HOC system there are indications of avoided crossings among the resonant states also

when the O-C coordinate is varied. By applying structure calculations we explore the angle dependence of the resonant states. The resulting potentials of ${}^2A'$ and ${}^2A''$ symmetries as a function of the bending angle, with $R_{HO}=2.0a_0$ and $R_{OC}=2.08a_0$ frozen, are displayed in Fig. 5. There is no strong angle dependence of the resonant states of HOC in the Franck-Condon region.

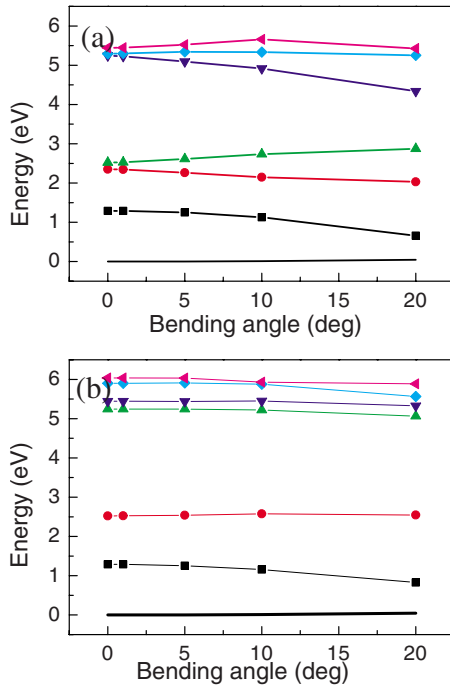


FIG. 5. (Color online) Resonant states of HOC of (a) $^2A'$ and (b) $^2A''$ symmetries as a function of the bending angle and for fixed radial coordinates ($R_{HO}=2.0a_0$ and $R_{OC}=2.08a_0$). Also the ground state, X^2A' , of the HOC^+ ion is shown with the solid curve.

The autoionization widths of the HOC resonant states at the geometry $R_{HO}=2.0a_0$, $R_{OC}=2.08a_0$, and $\theta=0^\circ$ are listed in Table II. As can be seen in Table II, at the equilibrium geometry, the lowest $1^2\Sigma^+$ resonant state has a large autoionization width. However, when the H-O coordinate increases, there are avoided crossings with the higher resonant states [see Fig. 5(a)], and the higher-lying resonant states will have the larger width. All the $^2\Pi$ resonant states have relatively small autoionization widths that do not strongly depend on changes in the radial coordinates. Also at the avoided crossings of the $^2\Delta$ resonant states [see Fig. 5(c)], the widths of the adiabatic resonant states are interchanged.

TABLE II. Autoionization widths of the resonant states of HOC at $R_{HO}=2.0a_0$, $R_{OC}=2.08a_0$, and $\theta=0^\circ$.

Resonant state	Autoionization width (eV)
$1^2\Sigma^+$	0.24
$2^2\Sigma^+$	0.021
$3^2\Sigma^+$	0.076
$1^2\Pi$	0.022
$2^2\Pi$	0.019
$3^2\Pi$	0.015
$4^2\Pi$	0.031
$1^2\Delta$	0.061
$1^2\Delta$	0.0017
$1^2\Delta$	0.018

IV. DISCUSSION

We have combined electron-scattering calculations with structure calculations to compute the electronic resonant states of HCO and HOC. In a second step, we are planning to perform dynamics calculations on these resonant states in order to examine the role of the electronic resonant states in DR of HCO^+ and HOC^+ .

For the HCO system, we find no resonant state that crosses the ion close to its minimum. The present study therefore supports the mechanism that the low-energy DR of HCO^+ is driven by the electron capture and dissociation through the Rydberg states situated below the ion. However, for electron energies above a few eV, there are a manifold of resonant states. Electron capture and dissociation through these resonant states will create a high-energy peak in the cross section as has been observed in the ion-storage ring experiment [22]. Since the resonant states are repulsive as a function of the two radial coordinates, but relatively flat as a function of the bending angle, it will be important to include at least two dimensions in the dynamics study. In DR of HCO^+ at low collision energies, only the H-C bond breaks. However, at higher energies, when these resonant states become important, both bonds may break.

Compared with HCO^+ much less is known about DR of HOC^+ . This ion has been observed in interstellar space [37–39] and the DR of this ion can be an important destruction mechanism. There are only speculations of the rate for DR of HOC^+ . This is as far as we know the first theoretical study of the electronic resonant states of HOC. We find several resonant states that cross the ion in the Franck-Condon region. We believe that these resonant states can play an important role in the DR reaction even at low collision energies. The resonant states are repulsive with respect to the two radial coordinates but relatively independent on changes in the bending angle. Again, at least two dimensions have to be included in the theoretical description of the dynamics for this reaction. In the low-energy DR of HOC^+ there can thus be larger probability for three-body breakup.

As mentioned above, in the experiments on DR of HCO^+ , it is difficult to distinguish the two isomers HCO^+ and HOC^+ . If a larger cross section for DR of HOC^+ compared to HCO^+ is found, this can help us to explain the discrepancy between the experimental and theoretical values for the DR cross section of HCO^+ at low energies. We hope that future studies can resolve these issues.

V. CONCLUSIONS

We have calculated electronic resonant states of HCO and HOC. The resonant states are repulsive with respect to the two radial coordinates, but relatively flat when the bending angle is varied. Furthermore, there are avoided crossings among bound and dissociative resonant states. These resonant states play an important role for dissociative recombination of the corresponding cations.

The resonant states of HCO do not cross the ground ionic potential-energy surface close to the equilibrium structure. Instead a few eV is needed to capture into these resonant

states and they will only be important for the cross section at higher energies.

The resonant states of HOC are much lower in energy compared to the ion and are crossing the ion potential close to the equilibrium geometry. A future study will examine if these states drives the low-energy DR of HOC⁺.

ACKNOWLEDGMENTS

We thank D. Haxton for helpful discussions. Å.L. acknowledges support from The Swedish Research Council and A.E.O. acknowledges support from the National Science Foundation Grant No. PHY-05-55401.

-
- [1] D. Buhl and L. E. Snyder, *Nature (London)* **228**, 267 (1970).
 [2] W. Klemperer, *Nature (London)* **227**, 1230 (1970).
 [3] T. Amano and T. Nakanaga, *Astrophys. J.* **328**, 373 (1988).
 [4] T. M. Millar, in *Molecular Astrophysics*, edited by T. W. Hartquist (Cambridge University Press, Cambridge, England, 1990), p. 115.
 [5] M. T. Leu, M. A. Biondi, and R. Johnsen, *Phys. Rev. A* **8**, 420 (1973).
 [6] R. C. Woods, T. A. Dixon, R. J. Saykally, and P. G. Szanto, *Phys. Rev. Lett.* **35**, 1269 (1975).
 [7] B. Ganguli, M. A. Biondi, R. Johnsen, and J. L. Dulaney, *Phys. Rev. A* **37**, 2543 (1988).
 [8] T. Amano, *J. Chem. Phys.* **92**, 6492 (1990).
 [9] N. G. Adams, D. Smith, and E. Alge, *J. Chem. Phys.* **81**, 1778 (1984).
 [10] N. G. Adams and D. Smith, *Molecular Astrophysics: State of the Art and Future Directions*, Proceedings of the NATO Advanced Workshop, edited by G. H. F. Diercksen *et al.* (Reidel, New York, 1985), p. 657.
 [11] N. G. Adams, C. R. Herd, M. Geoghegan, D. Smith, A. Canosa, J. C. Gomet, B. R. Rowe, J. L. Queffelec, and M. Morlais, *J. Chem. Phys.* **94**, 4852 (1991).
 [12] N. G. Adams and L. Babcock, *Astrophys. J.* **434**, 184 (1994).
 [13] B. R. Rowe, J. C. Gomet, A. Canosa, C. Rebrion, and J. B. A. Mitchell, *J. Chem. Phys.* **96**, 1105 (1992).
 [14] T. Gougousi, M. F. Golde, and R. Johnsen, *Chem. Phys. Lett.* **265**, 399 (1997).
 [15] J. M. Butler, L. M. Babcock, and N. G. Adams, *Mol. Phys.* **91**, 81 (1997).
 [16] S. Laubé, A. Le Padellec, O. Sidko, C. Rebrion-Rowe, J. B. A. Mitchell, and B. R. Rowe, *J. Phys. B* **31**, 2111 (1998).
 [17] V. Poterya, J. L. McLain, N. G. Adams, and L. M. Babcock, *J. Phys. Chem. A* **109**, 7181 (2005).
 [18] R. E. Rosati, M. P. Skrzypkowski, R. Johnsen, and M. F. Golde, *J. Chem. Phys.* **126**, 154302 (2007).
 [19] I. Korolov, R. Plasil, T. Kotrik, P. Dohnal, and J. Glosik, *Int. J. Mass. Spectrom.* **280**, 144 (2009).
 [20] A. Le Padellec, C. Sheehan, D. Talbi, and J. B. A. Mitchell, *J. Phys. B* **30**, 319 (1997).
 [21] W. D. Geppert, R. Thomas, A. Ehlerding, J. Semaniak, F. Österdahl, M. af Ugglas, N. Djurić, A. Paál, and M. Larsson, *Faraday Discuss.* **127**, 425 (2004).
 [22] W. D. Geppert *et al.* (private communication).
 [23] M. Larson and A. E. Orel, *Dissociative Recombination of Molecular Ions* (Cambridge University Press, Cambridge, England, 2008).
 [24] W. P. Kraemer and A. U. Hazi, *Molecular Astrophysics: State of the Art and Future Directions*, Proceedings of the NATO Advanced Workshop, edited by G. H. F. Diercksen *et al.* (Reidel, New York, 1985), p. 575.
 [25] W. P. Kraemer and A. U. Hazi, *Dissociative Recombination: Theory, Experiment and Applications* (World Scientific, Singapore, 1989), p. 62.
 [26] D. R. Bates, *Phys. Rev.* **78**, 492 (1950).
 [27] D. Talbi, F. Pauzat, and Y. Ellinger, *Chem. Phys.* **126**, 291 (1988).
 [28] D. Talbi, A. P. Hickman, F. Pauzat, Y. Ellinger, and G. Berthier, *Astrophys. J.* **339**, 231 (1989).
 [29] D. R. Bates, *J. Phys. B* **25**, 5479 (1992).
 [30] Å. Larson, S. Tonzani, R. Santra, and C. H. Greene, *J. Phys.: Conf. Ser.* **4**, 148 (2005).
 [31] I. A. Mikhailov, V. Kokoouline, Å. Larson, S. Tonzani, and C. H. Greene, *Phys. Rev. A* **74**, 032707 (2006).
 [32] N. Douguet, V. Kokoouline, and C. H. Greene, *Phys. Rev. A* **77**, 064703 (2008).
 [33] Ch. Jungen and S. T. Pratt, *J. Chem. Phys.* **129**, 164311 (2008).
 [34] N. Douguet, V. Kokoouline, and C. H. Greene (unpublished).
 [35] M. Mladenović and S. Schmatz, *J. Chem. Phys.* **109**, 4456 (1998).
 [36] C. S. Gudeman and R. C. Woods, *Phys. Rev. Lett.* **48**, 1344 (1982).
 [37] R. C. Woods, C. S. Gudeman, R. L. Dickman, P. F. Goldsmith, G. R. Huguenin, W. M. Irvine, Å. Hjalmorson, L.-Å. Nyman, and H. Olofsson, *Astrophys. J.* **270**, 583 (1983).
 [38] L. M. Ziurys and A. J. Apponi, *Astrophys. J.* **455**, L73 (1995).
 [39] H. Liszt, R. Lucas, and J. H. Black, *Astron. Astrophys.* **428**, 117 (2004).
 [40] The UMIST database; see www.udfa.net
 [41] T. N. Rescigno, C. W. McCurdy, A. E. Orel, and B. H. Lengsfeld III, in *The Complex Kohn Variational Method in Computational Methods for Electron-Molecule Scattering*, edited by W. H. Huo and F. A. Gianturco (Plenum, New York, 1995).
 [42] S. Geltman, *Topics in Atomic Collision Theory* (Academic Press, New York, 1997), p. 31.
 [43] J. M. L. Martin, P. R. Taylor, and T. J. Lee, *J. Chem. Phys.* **99**, 286 (1993).
 [44] Those interested in the numerical data for the potential-energy surfaces should contact the authors to obtain the data.